

Jitter Sensitivity Analysis of the Superconducting Josephson Arbitrary Waveform Synthesizer

Christine A. Donnelly¹, *Graduate Student Member, IEEE*, Justus A. Brevik¹, Paul D. Dresselhaus¹,
Peter F. Hopkins¹, *Member, IEEE*, and Samuel P. Benz¹, *Fellow, IEEE*

Abstract—We present the first jitter sensitivity analysis of a superconducting voltage reference waveform synthesizer with fundamentally accurate output pulses. Successful deployment of a reference waveform source at microwave frequencies will represent a new paradigm for radio frequency metrology. The programmable waveform synthesizer considered in this paper contains a 1.5 bit delta-sigma digital-to-analog converter (DAC) with a sampling frequency of 28 GHz. We quantify the impact of random and deterministic output pulse position jitter (PPJ) on: 1) the amplitude accuracy of the output fundamental tone and 2) the in-band signal-to-noise and distortion ratio (SNDR). The superconducting DAC features a complete lack of output pulsewidth jitter, and random PPJ up to 200 fs rms has a negligible impact on accuracy and SNDR for synthesized tones up to 1 GHz. However, application of nonzero dc bias current is shown to produce deterministic PPJ of up to 5 ps, which, in turn, is shown to degrade the in-band SNDR by 30 dB at 1 GHz unless eliminated with techniques discussed in this paper. We verify the predicted effects of random and deterministic PPJ with simulations in the range of 100 kHz–1 GHz and with experiments in the range of 100 kHz–3 MHz.

Index Terms—Delta-sigma modulation, digital-to-analog converter (DAC), jitter, Josephson junction (JJ), superconductivity.

I. INTRODUCTION

THE JOSEPHSON arbitrary waveform synthesizer (JAWS) is a superconducting digital-to-analog converter (DAC) used as the primary ac voltage standard in the audio-frequency spectrum [1], [2]. The JAWS system is assumed to be a “perfect” data converter, receiving a digital input pulse stream and outputting voltage pulses, each having a perfectly quantized and identical time-integrated area of exactly $h/2e$, where h is Planck’s constant and e is the electron charge.¹ Efforts have

begun at the National Institute of Standards and Technology (NIST) to experimentally demonstrate JAWS performance in the microwave-frequency range. JAWS waveform synthesis has recently been experimentally demonstrated at 100 MHz [4] with plans to extend to over 1 GHz. This paper contains a theoretical study of the effects of output pulse timing jitter, as JAWS is extended to microwave frequencies.

The JAWS system is one of the several superconducting circuit approaches for synthesizing voltage reference waveforms. An alternative approach uses a zero-order-hold (ZOH) Nyquist-rate superconducting DAC with quantized voltage steps rather than quantized pulse areas [5], [6]. With this latter approach, jitter in the level transition timing is shown to significantly degrade output accuracy for synthesis above several kilohertz [7], [8]. However, no parallel analysis of jitter sources and jitter sensitivity has yet been reported for JAWS circuits. In this paper, we simulate the JAWS bias signals and device physics to identify mechanisms for pulse position jitter (PPJ) and to quantify the frequency-dependent effects of jitter on JAWS accuracy and spectral purity.

Jitter in conventional DACs is a limiting factor for achieving high spurious free dynamic range (SFDR) and signal-to-noise and distortion ratio (SNDR) [9], [10] and arises from sources such as sampling clock phase noise and intersymbol interference (ISI) [11], [12]. The deviation from ideal DAC output is often categorized into errors in pulse position or errors in pulsewidth [13].

When timing jitter is random and white, pulsewidth jitter (PWJ) has the most detrimental effect on in-band noise metrics, because the noise contributed by PPJ is shaped to high frequencies that are typically out of band [14], [15]. For this reason, many designers of nonsuperconducting DAC architectures report extensive efforts to minimize PWJ [16], [17], even at the expense of degraded linearity and increased circuit complexity [15], [18]. When jitter is deterministic, PPJ and PWJ both generate harmonics and spurious tones that degrade in-band noise and distortion metrics [19].

Due to the quantized nature of JAWS output pulse areas, the JAWS system features an intrinsic lack of PWJ in the output pulses; we will show that this leads to superior sensitivity to random timing jitter compared to conventional DAC architectures. However, we have identified and measured a physical mechanism of the JAWS system that causes deterministic PPJ, which has not been previously observed or explained. We report our experimental findings of this deterministic PPJ

Manuscript received April 16, 2018; accepted July 2, 2018. Date of publication August 9, 2018; date of current version November 5, 2018. The work of C. A. Donnelly was supported by the National Institute of Standards and Technology under a GMSE Fellowship. (*Corresponding author: Christine A. Donnelly.*)

C. A. Donnelly is with the Superconductive Electronics Group, National Institute of Standards and Technology (NIST), Boulder, CO 80305 USA, and also with the Department of Electrical Engineering, Stanford University, Stanford, CA 94305 USA (e-mail: cdonnelly@stanford.edu).

J. A. Brevik, P. D. Dresselhaus, P. F. Hopkins, and S. P. Benz are with the Superconductive Electronics Group, National Institute of Standards and Technology (NIST), Boulder, CO 80305 USA (e-mail: justus.brevik@nist.gov; paul.dresselhaus@nist.gov; peter.hopkins@nist.gov; samuel.benz@nist.gov).

Color versions of one or more of the figures in this paper are available online at <http://ieeexplore.ieee.org>.

Digital Object Identifier 10.1109/TMTT.2018.2856775

¹The ratio of $h/2e$ will become an exact value in May 2019 based on the approved exact values for h and e as part of the redefinition of the International System of Units (SI) [3].

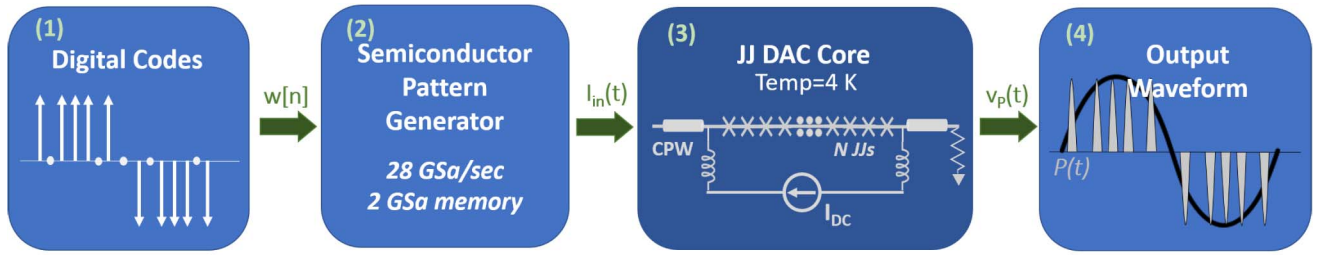


Fig. 1. Schematic of the JAWS system. 1: input $w[n]$ is a three-level delta-sigma encoding of a target output waveform. 2: room-temperature pattern generator synthesizes a series of three-level current pulses based on the programmed digital encoding. 3: input current waveform $I_{in}(t)$ is transferred to a cryogenic superconducting JAWS chip that contains an array of JJs (symbolized by an “X” in circuit diagrams), and that transforms the input current pulses to output voltage pulses with quantized area. 4: output waveform $v_P(t)$, consisting of a train of JAWS-synthesized pulses, is measured at room temperature using a digitizer or spectrum analyzer, or is used as input to a device under test.

and show excellent corroboration between the measured results and model calculations and simulations. We also suggest methods to eliminate this deterministic PPJ so as to preserve spectral purity for programmable synthesized microwave frequencies.

This paper is organized as follows. In Section II, we provide an overview of the JAWS system architecture and its component superconducting devices. In Section III, we discuss deterministic PPJ in the JAWS system. In Section IV, we discuss random output pulse jitter in the JAWS system. Discussion is presented in Section V, and our conclusions are given in Section VI.

II. JAWS DEVICE OPERATION

A. Operational Description

A schematic of the JAWS circuit is shown in Fig. 1. The JAWS DAC converts three-level (1.5 bit) digital encodings of target waveforms into three-level output streams of pulses with quantized area, such that the positive and negative pulses plus the zero pulse condition produce synthesized waveforms of bipolar amplitude. First [see Fig. 1 (Box 1)], an arbitrary waveform is encoded into a three-level $(-1, 0, +1)$ bitstream, here called $w[n]$. We use a low-pass or bandpass delta-sigma encoding algorithm to move the quantization noise out of band [15]. The bitstream $w[n]$ is stored in the memory of a room-temperature pattern generator. The JAWS system can also be operated as a 1 bit DAC with a two-level (unipolar) $w[n]$ sequence.

At operation, the pattern generator converts $w[n]$ to an input current waveform I_{in} [see Fig. 1 (Box 2)]. For the experiments described in this paper, we use a Keysight M8195A arbitrary waveform generator² with a clock rate of 28 GHz and an analog bandwidth of 25 GHz.

The waveform I_{in} is transferred, via coaxial cables embedded in a cryogenic probe, to the superconducting JAWS chip that resides at a temperature of ~ 4 K in liquid helium [see Fig. 1 (Box 3)]. The JAWS chip, which serves as the DAC core, contains a series-connected array of superconducting

circuit elements known as Josephson junctions (JJs). The JJs are embedded in the center conductor of a coplanar waveguide. The current I_{in} provides the microwave-frequency input excitation, while I_{dc} is a tunable dc offset current. Most implementations of the JAWS system include additional digital code prefiltering and on-chip analog filtering to isolate the measured output waveform from the input drive; the details of the circuit design and pulse drive are described elsewhere [20].

In response to the input multibit bias signal, the JJs create the waveform $v_P(t)$ by producing output pulses that match the encoded polarity of the digital bitstream [see Fig. 1 (Box 4)]. For a specific range of input parameters, the DAC core operates in “quantum-locked” conditions, in which there is one output pulse per JJ per input pulse, and the voltage area of each output pulse is equal to $h/2e$. The area of every quantized pulse is completely invariant with respect to I_{in} , I_{dc} , or any other environmental or experimental variables. All the experimental measurements and analyses presented in this paper assume that the JAWS device is operating in quantum-locked conditions. This quantum-locked behavior is what produces the voltage accuracy and waveform purity of the JAWS device output signals. It distinguishes the JAWS DAC from all other DACs.

In the absence of jitter, the DAC output waveform $v_P(t)$ is described by the convolution of the output pulse $P(t)$ from the full JJ array with the input digital bitstream

$$v_P(t) = P(t) \otimes \sum_n w[n] \delta(t - nT) \quad (1)$$

where the symbol \otimes refers to convolution, T is the sampling period defined by the pattern generator, t refers to time, and n is the bit index of the input bitstream $w[n]$.

B. DAC Core and Josephson Junctions

The JJs in the JAWS DAC core each consist of two niobium superconducting electrodes, separated by a thin barrier of nonsuperconducting material. In this paper, we deal with junctions that have a noninsulating $\text{Nb}_x\text{Si}_{1-x}$ junction barrier [21]. These JJs have negligible capacitance and are well described by the resistively shunted junction (RSJ) model [22]. The RSJ model is shown in Fig. 2(a). In this model, input excitation current splits between a resistive current branch and

²Commercial instruments are identified in order to adequately specify the experimental procedure. Such identification does not imply recommendation or endorsement by NIST, nor does it imply that the equipment identified is necessarily the best available for the purpose.

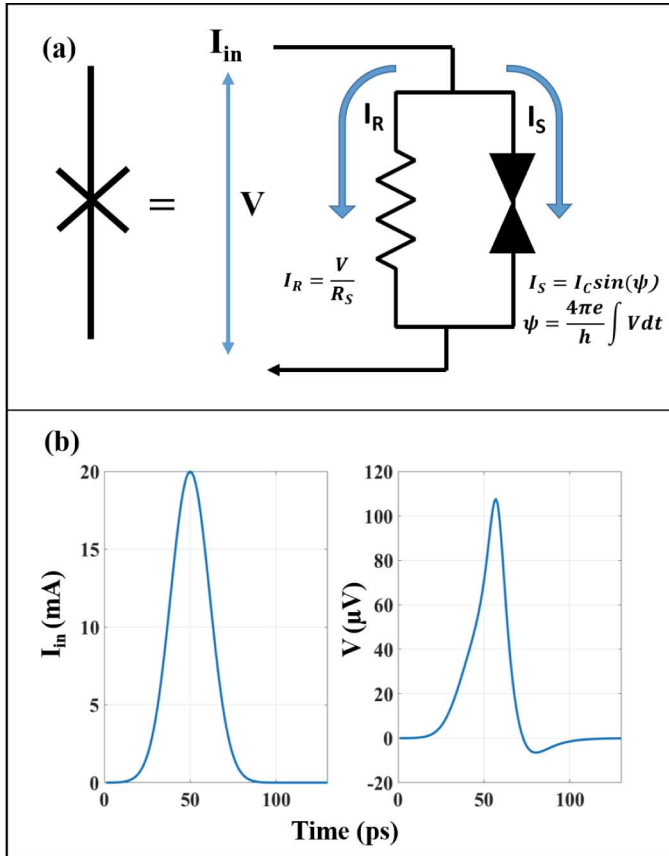


Fig. 2. (a) RSJ model of a JJ: the device (symbolized by an “X”) is modeled as a resistor (R_S) in parallel with a superconducting current branch. (b) Output voltage pulse waveform (right) from a single JJ in response to an input current pulse (left). The time integral of $V(t)$ is exactly $h/2e$.

supercurrent branch. The supercurrent branch can pass a maximum dc current of I_c , known as the critical current. The resistance (R_S) and I_c are adjustable by the selection of barrier and superconductive electrode materials and by fabrication parameters, such as barrier thickness, niobium concentration, and junction area. The JJs used for this paper are modeled with $R_S = 4.5 \text{ m}\Omega$ and $I_c = 7.2 \text{ mA}$, which are the mean values of the experimentally measured JJs in the arrays. The characteristic pulse time of the JJs decreases with increasing $I_c R_S$ product.

The current–voltage characteristics of the JJs are given by the Josephson equations [22]

$$I_S = I_c \sin(\psi) \quad (2)$$

$$\psi = \frac{4\pi e}{h} \int V dt \quad (3)$$

where I_S is the current through the supercurrent branch and ψ is the junction phase. An external dc input current below I_c is fully shunted by the supercurrent branch, while a time-varying input or an input greater than I_c forces a time-varying potential difference $V(t)$ across the junction.

When a JJ is in the quantum-locked conditions, a transient driving current pulse causes the junction phase (proportional to integrated voltage) to change by 2π , as current through the superconducting branch evolves through one period of

$I_{dc} = I_c \sin(\psi) \rightarrow I_{dc} = I_c \sin(\psi + 2\pi)$. The 2π change in the junction phase corresponds to an integrated voltage pulse area of $\int V dt = h/2e$. This is known as a single flux quantum (SFQ) pulse. Examples of an input current drive pulse and an output SFQ pulse are shown in Fig. 2(b).

Because the quantized pulse area given by a single junction is small, the JAWS system uses a series array of N nominally identical JJs, so that the area of the output response is $Nh/2e$ for each input pulse to the array. Single-tone waveforms with rms amplitude up to 2 V have been demonstrated at 1 kHz, using 102,400 JJs in series [23].

For the simulation of JJ dynamics and interactions with other circuit elements, we use a version of SPICE [24] that implements the RSJ JJ model.

C. Relevant System Metrics

The JAWS system is used in a variety of applications, including calibration of rms power within a specified bandwidth, calibration of single-tone and multitone amplitudes, and characterization of nonlinear effects in transmitter and receiver chains and measurement electronics [25], [26]. In particular, the perfect linearity of the programmable output amplitudes is a unique feature of the JAWS system, as is the ability to synthesize multitone signals with stable, repeatable amplitudes and arbitrary ratios. Only single-tone waveforms are considered in this paper and we use the following two metrics to quantify accuracy and spectral purity of these tones.

1) *Fundamental Tone Accuracy*: The amplitude accuracy of the fundamental tone is defined as any deviation of the output fundamental amplitude from the value programmed in $w[n]$. Currently, the state-of-the-art radio frequency (RF) calibration services based on thermal converters offer an uncertainty of $100 \mu\text{V/V}$ – $1000 \mu\text{V/V}$ at 1 MHz, and thermistor-referenced power calibrations have a flat uncertainty metric of $2000 \mu\text{V/V}$ for 10 MHz–1 GHz [27]. We expect the fully developed JAWS system to outperform these metrics. The JAWS system also offers the advantage of spectral selectivity, whereas thermistor-based systems can only integrate the total output power from an RF source.

2) *SNDR*: We define SNDR in this paper as the ratio of signal power to total noise and distortion power within a $\pm 5 \text{ MHz}$ bandwidth of the fundamental tone f_0 , expressed in decibel units. We chose this bandwidth, because the simulations of bandpass delta–sigma encodings described in this paper use a bandwidth of 10 MHz. For $f_0 < 5 \text{ MHz}$, we integrate noise power from dc to 10 MHz to calculate SNDR.

We use delta–sigma waveform encodings in this paper that have in-band signal-to-quantization-noise ratio (SQNR) of at least 80 dB. Noise and distortion contributed by jitter will ideally remain below the quantization noise level.

III. DETERMINISTIC PULSE POSITION JITTER

A. Sources of Deterministic PPJ

1) *Nonzero DC Current*: The main source of deterministic jitter considered in this paper is polarity-dependent shift in the output pulse timing due to a nonzero I_{dc} through the JJ array.

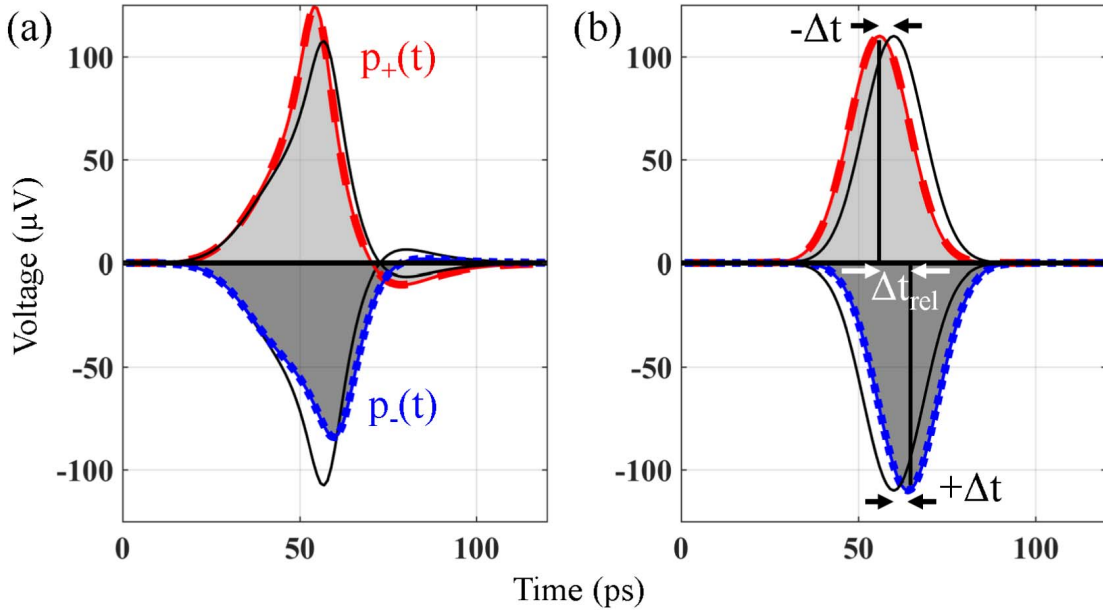


Fig. 3. (a) Voltage-time traces of positive (coarse dashes) and negative (fine dashes) SFQ pulses with positive applied bias, I_{dc} , based on a SPICE model of a single JJ with $I_c = 7.2$ mA and $R_J = 4.5$ m Ω . The shaded area of each pulse is $h/2e$. (b) Simplified PPJ model for the difference between $p_+(t)$ and $p_-(t)$. In this model, differences between the pulse shapes due to $I_{dc} \neq 0$ are neglected. In both figures, the black solid curves show the shapes of positive and negative pulses when $I_{dc} = 0$.

When $I_{dc} = 0$, each input pulse causes a phase winding of each JJ, from $\psi = 2\pi x \rightarrow \psi = 2\pi(x + 1)$. However, if $I_{dc} \neq 0$, the JJ phase will instead proceed from $2\pi x + \psi_0 \rightarrow 2\pi(x + 1) + \psi_0$. According to the dc Josephson equation, $\psi_0 = \sin^{-1}(I_{dc}/I_c)$.

Within the quantum locking range, the constant offset ψ_0 does not affect the quantized SFQ pulse area. It was, therefore, previously assumed that the output waveform variation with respect to I_{dc} should be identically zero [2]. However, we have recently experimentally observed I_{dc} -dependent harmonic generation, which indicates that while variations in I_{dc} do not affect the SFQ pulse area, they do lead to deterministic, polarity-dependent jitter in the SFQ pulse position. SPICE simulations of positive and negative SFQ pulse waveforms from a single JJ ($p_+(t)$ and $p_-(t)$) with a positive I_{dc} are shown in Fig. 3(a). The symmetry between positive and negative pulse waveforms is broken when $I_{dc} \neq 0$.

The detailed differences between the shapes of $p_+(t)$ and $p_-(t)$ observed in Fig. 3(a) are neglected in our model of PPJ. The simplified PPJ model uses a fixed relative time shift between opposite polarity pulses and ignores I_{dc} -dependent differences in pulse shape, as shown in Fig. 3(b).

The relative time shift Δt_{rel} is determined by the relative phase delay between pulses, $\Delta t_{rel} = (\Delta\phi(f)/2\pi f)$, where $\Delta\phi(f)$ is the phase shift between the Fourier components of $p_+(t)$ and $p_-(t)$ at frequency f . The pulses shown in the model of Fig. 3(b) have constant relative phase delay at all frequencies. The actual JJ pulses shown in Fig. 3(a) have frequency-dependent phase delay above 1 GHz. As shown in Section III-C, our PPJ model becomes inaccurate above 1 GHz, because it does not include this dispersion effect.

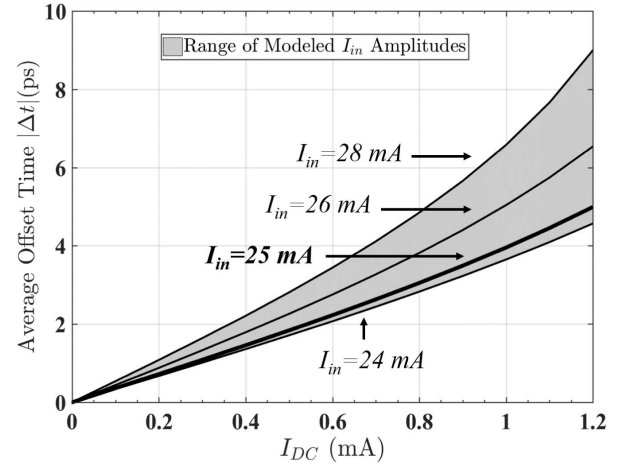


Fig. 4. Various $|\Delta t|$ versus I_{dc} curves for different I_{in} microwave amplitudes. The curve used for SPICE simulations in this paper is indicated with a thick black line.

For the PPJ model, we define $\Delta t = \pm \Delta t_{rel}/2$; this is the advance or delay of a positive or negative pulse when $I_{dc} \neq 0$ relative to its position when $I_{dc} = 0$. In Fig. 4, $|\Delta t|$ is plotted as a function of I_{dc} based on SPICE simulations of the JJs. In general, a pulse with polarity that matches the polarity of I_{dc} will experience a slight advance in time ($\Delta t < 0$), and a pulse with opposite polarity to I_{dc} will be delayed ($\Delta t > 0$). The value of Δt is also sensitive to the input pulse amplitude I_{in} , which is tuned in experiments to maximize the quantum locking range. The Δt -versus- I_{dc} curves for several I_{in} values are shown in Fig. 4. The curve corresponding to I_{in} pulse amplitude of 25 mA was used for all modeling in

this paper. The JAWS system fails to remain quantum locked at $|I_{dc}| \gtrsim 1.2$ mA. The value of Δt grows nonlinearly with I_{dc} near this failure condition, as the SFQ pulse shapes become increasingly distorted relative to their shape at $I_{dc} \neq 0$.

2) *Other Sources of Deterministic PPJ*: At the chip level, nonzero I_{dc} is expected to be the dominant source of jitter that causes deterministic pulse timing errors. However, the room-temperature input pulse drive electronics are another potential source of deterministic PPJ. For example, deviations from the ideal 50% eye crossing percentage in the input RF amplifier will cause polarity-dependent asymmetry in the input pulse drive. Similar to nonzero I_{dc} , this would cause timing offsets between positive and negative output pulses. The eye crossing level of the amplifier is tuned to maximize the quantum locking range prior to JAWS operation.

We use a return-to-zero scheme for the input pulse drive to minimize ISI, which may cause code-density-dependent timing differences in output pulses. However, some ISI may still result in high-amplitude, high-pulse-density input codes. ISI could also arise from attenuation and dispersion of the input pulse drive caused by the input cabling.

In our experimental measurements up to 3 MHz, nonzero I_{dc} is the only source of deterministic PPJ to cause observable deviation between the programmed and the expected output spectrum.

B. Theoretical Effect of Deterministic PPJ

In this section, we use the deterministic PPJ model to simulate trends in amplitude accuracy and SNDR; equations are derived in the Appendix. According to the deterministic PPJ model, the output waveform from the JAWS system can be expressed as the convolution of the JJ array pulse waveform with the time-shifted digital input encoding

$$v_{P,jit}(t) = P(t) \otimes \sum_n w[n] \delta(t - nT + \Delta t(I_{dc})w[n]) \quad (4)$$

where the magnitude of the time shift $\Delta t(I_{dc})$ is chosen according to the indicated mapping in Fig. 4, and the polarity depends on the polarity of the pulse, encoded in $w[n]$. Simulations of (4) can be performed quickly and do not require analog circuit modeling, because all changes in the output pulses are transferred to time shifts in the input digital code.

To the first order, deterministic polarity-dependent PPJ as defined in (4) causes mixing of the spectrum of the jitter-free waveform $v_P(t)$ with itself. The spectral content of $v_P(t)$ includes both the fundamental tone f_0 and the digital encoding quantization noise. Mixing generates spurious content at all possible sum and difference frequencies; these deterministic spurs cannot be reduced by longer data acquisition times or averaging. The spurious content results in a loss in amplitude of the programmed tone, thus compromising the expected JAWS voltage accuracy.

The effect of deterministic, polarity-dependent PPJ on the original complex magnitude a_m of a tone at frequency f_m in the jitter-free output spectrum is overall expressed as

$$a_m \xrightarrow{\text{jitter}} (1 - \alpha(f_m))a_m \pm \Delta_{a,m}. \quad (5)$$

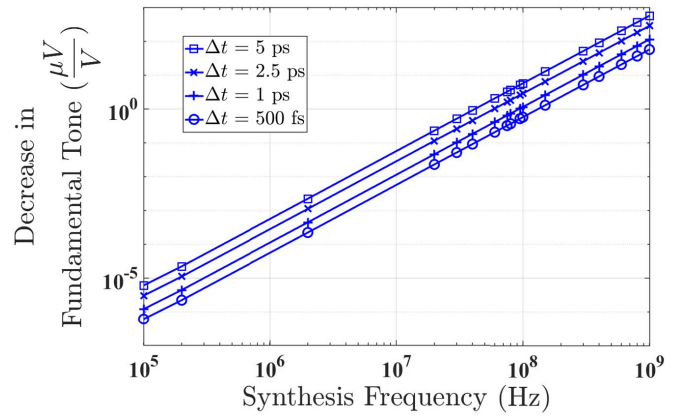


Fig. 5. Decrease in amplitude of the fundamental tone f_0 , as a function of frequency, for various deterministic jitter pulse offset times.

The first term $(1 - \alpha(f_m))a_m$ is a fractional decrease in amplitude, and dominates at the fundamental tone f_0 , and leads to indeterminate deviation from the programmed output value. The second term $\Delta_{a,m}$ is the net result of all quantization noise mixing that generates spurious content at f_m and is dominant in magnitude for frequencies $f_m \neq f_0$ within the delta-sigma encoding low-noise bandwidth.

1) *Amplitude Loss Due to Deterministic PPJ*: The fractional loss in the amplitude of the fundamental tone f_0 due to deterministic, polarity-dependent PPJ is approximately equal to (see the Appendix)

$$\alpha(f_0) = 1 - \prod_{f_m} (J_0(a_m 2\pi \Delta t f_0)) \quad (6)$$

where $J_0(x)$ is the Bessel function of the first kind, and the product is taken over all frequency components f_m in the ideal output $v_P(t)$. The loss in amplitude grows with f_0 , because $J_0(x)$ decreases below one as its input argument grows.

In Fig. 5, the simulated loss in the amplitude of the fundamental tone f_0 versus frequency is shown for a range of pulse offset times Δt . While this loss is calculable for a known Δt , the experimentally observable parameter is I_{dc} and not Δt . Any uncertainty in I_{dc} or the I_{dc} -versus- Δt relationship will thus lead to uncertainty in the output amplitude of the JAWS system. However, even at 1 GHz, Fig. 5 shows that the loss in amplitude is $<1000 \mu\text{V/V}$, and JAWS remains competitive with existing thermistor-referenced ac standards over the expected range of I_{dc} .

2) *Loss in SNDR Due to Deterministic PPJ*: Deterministic jitter degrades the SNDR metric when the average magnitude of $\Delta_{a,m}$ within the delta-sigma encoding low-noise bandwidth exceeds the average baseline quantization noise magnitude. The trend in $\Delta_{a,m}$ is on average linear with both frequency f_m and pulse time offset Δt (see the Appendix).

The simulated scaling of SNDR with frequency for an eighth-order bandpass encoding algorithm of total length 5 million samples (MSa) is shown in Fig. 6, at multiple values of Δt . The SNDR shown is the ratio of signal to jitter noise only, after subtracting out quantization noise. The minimum target SQNR of 80 dB is indicated. The scaling

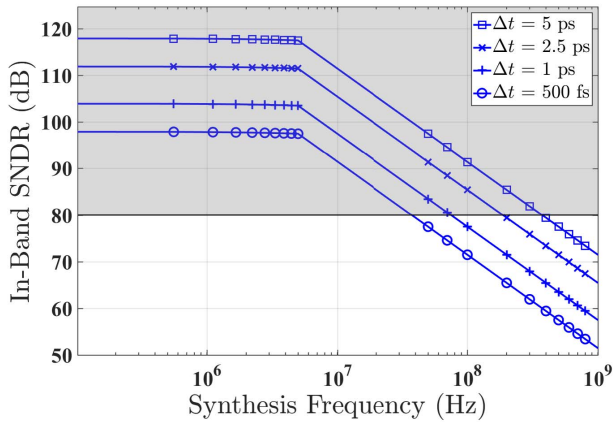


Fig. 6. Scaling of in-band SNDR due to deterministic jitter-contributed noise versus f_0 for deterministic pulse jitter times of $\Delta t = 500$ fs, 1 ps, 2.5 ps, and 5 ps. The baseline SQNR of 80 dB at $I_{dc} = 0$ is also shown. A 1.5 bit delta sigma code and 28 GHz clock frequency was used for this plot. Below 5 MHz, the SNDR is constant, because a fixed 10 MHz bandwidth was assumed.

of jitter-contributed SNDR with frequency is constant below $f_0 = 5$ MHz due to our definition of a 10 MHz noise bandwidth.

3) *Generation of the Second Harmonic:* Because polarity-dependent PPJ causes mixing of the spectrum of $v_P(t)$ with itself, a strong second harmonic signal is generated at $2f_0$ when $v_P(t)$ is a single-tone waveform. This will degrade SFDR for $f_0 < 5$ MHz, when $2f_0$ is within the delta-sigma code bandwidth.

Simulations with two-tone (f_1 and f_2) delta-sigma codes with $I_{dc} \neq 0$ show that the in-band third-order mixing product (e.g., at $2f_1 - f_2$) is small in amplitude compared to the second-order mixing products, and not expected to further degrade in-band noise and distortion metrics.

C. Verification of Theoretical Results

1) *JAWS Analog Circuit Simulations:* We use SPICE simulations to verify that the deterministic PPJ model of (4) is accurate up to 1 GHz, and to quantify inaccuracies of this model at higher frequencies.

A generic formulation for the effect of deterministic jitter that allows the pulse waveform to vary with each input bit can be written as

$$v_{P,\text{jit}}(t) = \sum_n P_n(t) \otimes w[n]\delta(t - nT). \quad (7)$$

This model, in which the output pulses depend on the code index n , is best implemented with full circuit simulations. In these simulations, we excite an array of 100 JJs with an input current waveform I_{in} that is generated based on a 1.5 bit bandpass delta-sigma encoding clocked at 28 GHz and is prefiltered based on the scheme described in [20]. We calculate the in-band SNDR of the resulting output waveform when $I_{dc} \neq 0$. In the reported simulations, we set $I_{dc} = 500 \mu\text{A}$. In the simplified model of (4), we use $\Delta t \approx 1.8$ ps, which corresponds to $I_{dc} = 500 \mu\text{A}$.

In Fig. 7, the jitter-contributed SNDR of the SPICE output waveform is compared to the computed SNDR, when fixed, polarity-dependent 1.8 ps bit shifts are applied to the delta-sigma code according to the PPJ model. SPICE simulations indicate that at frequencies above 1 GHz, SNDR due to $I_{dc} \neq 0$ remains higher than that predicted by (4). This trend is expected, because in reality the magnitude of the relative phase delay used to define Δt decreases below 1.8 ps at frequencies between 1 and 3 GHz.

SPICE simulations also reveal an amplitude loss of nearly 10,000 $\mu\text{V}/\text{V}$ at 1 GHz even when $I_{dc} = 0$, which is far greater than the incremental amplitude loss contributed by nonzero I_{dc} . We observe this deviation between the programmed amplitude and simulated output amplitude because, according to (1), the encoded spectrum of $w[n]$ is scaled by the spectrum of $P(t)$ at the JAWS output. The quantized pulse area in the time domain means that the $f = 0$ component of the pulse spectrum $[P(f)]$ is also quantized. The spectrum is flat and remains equal to its $f = 0$ value up to hundreds of megahertz, but rolls off at higher frequency. Because this roll-off has not been calibrated, it represents a source of additional uncertainty. The uncertainty can be reduced with the calibration measurements of the pulse spectrum $P(f)$ and with the use of JJs that have shorter characteristic pulse time (i.e., higher $I_c R_s$).

2) *Experimental Verification up to 3 MHz:* Generation of a second harmonic tone due to nonzero I_{dc} was experimentally observed for single-tone waveforms in the 100 kHz–3 MHz frequency range. The superconducting JAWS chip used in these experiments was fabricated at the NIST Boulder Micro-fabrication Facility using a niobium-silicon process. The JAWS chip contained an array of $N = 5100$ series-connected JJs. The chip was placed in a cryogenic-compatible measurement probe and immersed in liquid helium at ~ 4 K. The voltage across the array was measured with a 15 MSa/s digitizer, which limited experimental values f_0 to < 3.75 MHz so that the second harmonic would remain below the Nyquist frequency. After tuning the JAWS system input parameters to maximize the quantum locking range, I_{dc} was stepped from -1.5 to 1.5 mA, and 1000 time traces, each spanning 1000 periods of the synthesized sinusoid, were acquired and averaged in the frequency domain. We synthesized low-voltage output waveforms with an amplitude of 19.7 mV. Further details on the experimental setup and process are provided in [20].

The nonlinearity of the digitizer produced a strong second harmonic in the output data, even when $I_{dc} = 0$. The incremental second harmonic tone that was produced due to deterministic PPJ at $I_{dc} \neq 0$ added vectorially to this preexisting digitizer spur. To extract the I_{dc} -dependent portion of the data, we subtracted the phase and magnitude of the measured second harmonic at $I_{dc} = 0$ from the measured phase and magnitude of the second harmonic at all other bias points. The remaining I_{dc} -dependent portion of the data had magnitude and phase that were well matched to simulations. A comparison between the experimental and simulated phase and magnitude of the I_{dc} -dependent second harmonic signal is shown in Fig. 8 for a 100 kHz fundamental tone.

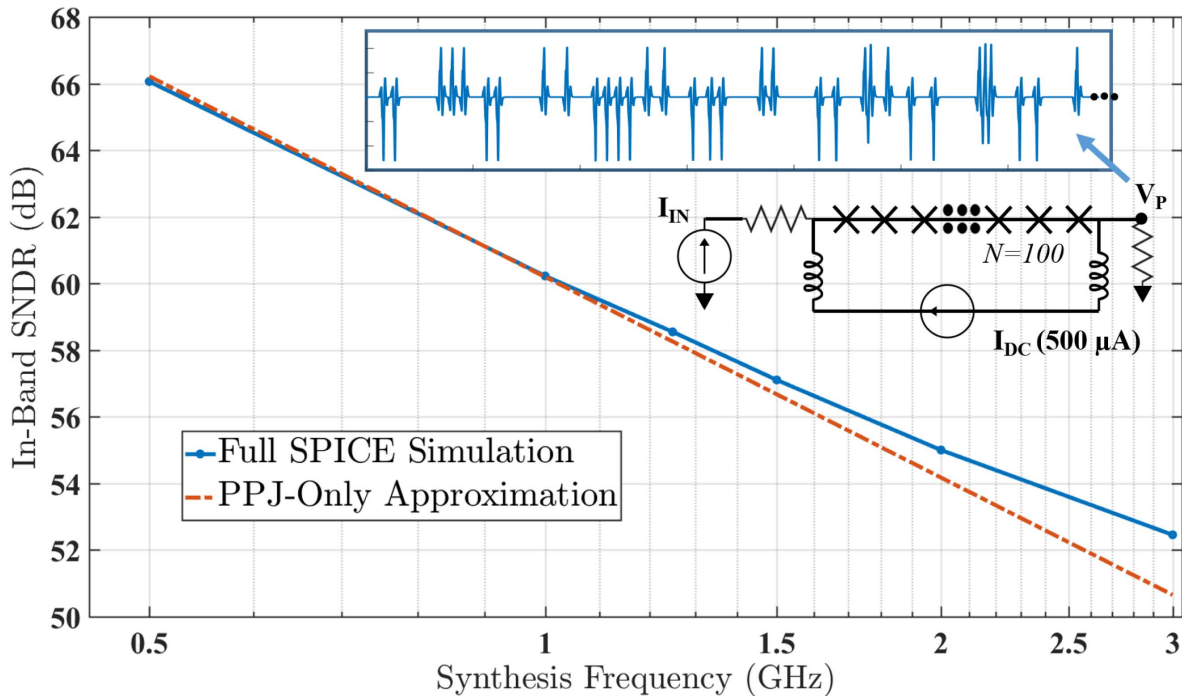


Fig. 7. Comparison of simulated jitter-contributed in-band SNDR for the simplified deterministic PPJ model with $\Delta t = 1.8$ ps versus a full SPICE simulation when $I_{dc} = 500 \mu\text{A}$, for synthesized tones in the range of 500 MHz–3 GHz. The 100-JJ circuit diagram used in SPICE and a sample of the output waveform are also shown.

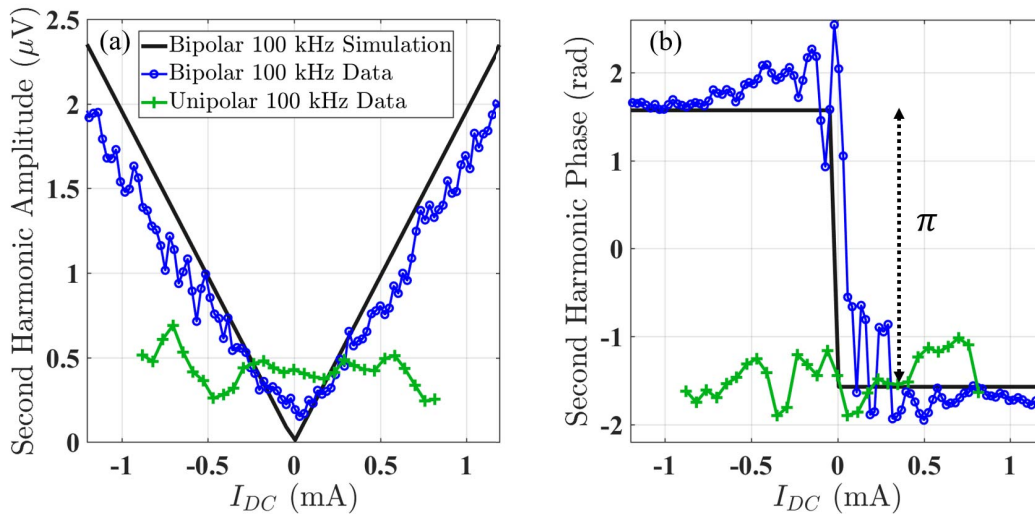


Fig. 8. (a) Measured (open circle) versus simulated (solid line) second harmonic amplitude versus bias current for a synthesized signal at $f_0 = 100$ kHz with a bipolar input encoding. Also shown are the I_{dc} -dependent experimental data with a unipolar input encoding (small crosses). (b) Measured versus simulated second harmonic phase versus bias current for a synthesized signal at $f_0 = 100$ kHz with a bipolar encoding, and measured second harmonic phase with a unipolar encoding.

Polarity-dependent, deterministic PPJ affects the spectrum of the output waveform, because we use *bipolar* delta sigma encodings. If we instead used a *unipolar* (0, +1) encoding scheme, a nonzero I_{dc} would cause a uniform advance (or delay) of all pulses, which would not distort the output waveform but would reduce the output amplitude by a factor of two. This may be a necessary step to eliminate PPJ in the design of JAWS circuits for RF calibration systems. In Fig. 8, we also show the trends in the second harmonic amplitude

and phase with I_{dc} for a 1 bit, *unipolar* 100 kHz waveform encoding, over the quantum locking range. The absence of any observable dependence on I_{dc} confirms that the second harmonic generation depends on the bipolarity of the input pulses.

Finally, when using bipolar waveform encodings, the experimental frequency dependence of the I_{dc} -dependent second harmonic slope ($\mu\text{V}/\text{mA}$) with bias current also matches simulation results. In Fig. 9, a comparison between the

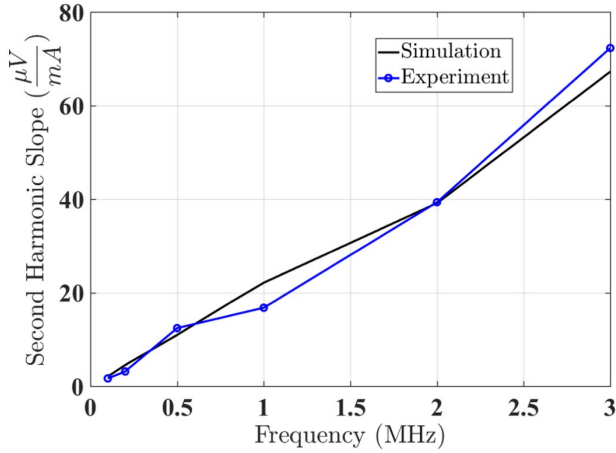


Fig. 9. Simulated and measured slope of the second harmonic amplitude at 1 mA bias current, as a function of frequency. Measurements were performed at 4 K, and the same chip was measured for this plot and for Fig. 8.

measurement and simulation of the slope of the second harmonic at 1 mA bias current is shown for a range of synthesis frequencies. We normalized the slopes of both the experimental and simulation data to the amplitude of f_0 . The simulations use the mapping of Δt -versus- I_{dc} that is shown in Fig. 4, and no additional free parameters are varied.

IV. RANDOM JITTER

As mentioned previously, the quantized-area JAWS output pulses do not have PWJ, and random timing jitter only leads to PPJ. In this section, we quantify the impact of random PPJ on the SNDR and on the amplitude of the fundamental tone f_0 . We compare these impacts with the effects of random timing jitter on ZOH DAC systems subject to PWJ, which was analyzed in [28] and [29].

A. Sources of Random Jitter

The dominant sources of random PPJ in the JAWS system are the input pattern generator and the input waveform amplifier. Based on specifications for the full chain of input electronics, we estimate an overall rms random jitter in the output pulses of 200–300 fs.

Random PPJ due to thermal noise in the cryogenic superconducting circuit components is negligible compared to noise from the room temperature input electronics [30], [31].

B. Theoretical Effect of Random Jitter

We use the following model for JAWS output in the presence of random PPJ:

$$v_{P,jit}(t) = P(t) \otimes \sum_n w[n] \delta(t - nT - \hat{e}_n) \quad (8)$$

where \hat{e}_n represents the random timing jitter and is assumed to be white, and its amplitude has a Gaussian distribution with a mean of zero and standard deviation σ .

In contrast, the PWJ that affects ZOH DACs is analyzed in [29] according to the model

$$v_{zoh}(t) = u(t) \otimes \sum_n \Delta w[n] \delta(t - nT_s - \hat{e}_n) \quad (9)$$

where $u(t)$ is the unit step function and $\Delta w[n] = w[n] - w[n-1]$. We derive the effects of random timing jitter for the JAWS system by repeating the derivations in [29], with the noise model in (8) substituted in place of the model in (9).

In Fig. 10(a), a sample ZOH DAC output signal subjected to random jitter is broken into a summation of ideal output and error signal.

The PPJ-perturbed JAWS output signal is also shown in Fig. 10(b) as a summation of an ideal signal and an error signal. Unlike for a ZOH DAC, the integrated area of the error signal is always zero over the time scale of a single output pulse. This feature has a high-pass filtering effect on the power spectral density (PSD) of the error signal [15].

For both JAWS and a ZOH DAC, the PSD of the jittered output is a sum of the PSD of the ideal signal, the PSD of the error signal, and a cross correlation term. The cross correlation term in the PSD of the jittered output results in loss in power from the fundamental tone. Power is redistributed into the continuous-frequency noise PSD of the error signal.

1) *Decrease in Amplitude of Fundamental Tone:* For both the JAWS system (subject to PPJ) and ZOH DACs (subject to PWJ), the fractional decrease in amplitude of the fundamental tone f_0 is given by [29]

$$0 < (|C(f_0)| - 1) < 1 \quad (10)$$

where $|C(f_0)| = e^{-(1/2)(2\pi f_0 \sigma)^2}$ for the timing noise model used in this paper.

This fractional decrease in amplitude is shown in Fig. 11 at a range of σ . We expect that random jitter in the JAWS system is ~ 250 fs. Given this jitter magnitude, the decrease in amplitude at 1 GHz is ~ 1 ppm and within an acceptable error range for the JAWS system.

2) *Noise Error Power Spectrum:* To calculate in-band SNDR in the presence of random noise, we integrate the noise PSD over a 10 MHz bandwidth that is centered at the fundamental tone. The closed-form expressions for SNDR given below assume that $\text{PSD}(f)$ varies negligibly over the narrow 10 MHz bandwidth so that $\text{PSD}(f) \approx \text{PSD}(f_0)$ in the range $f = f_0 \pm 5$ MHz. Full integrals of PSD were computed for Fig. 12.

For the JAWS DAC, we find that

$$\text{SNDR}(f_0) \approx 10 \log_{10} \left(\frac{2\text{OSR}}{A(1 - |C(f_0)|^2)} \right) \quad (11)$$

where A is the dimensionless ratio of total power in the delta-sigma code to power in the fundamental tone (typically 9–10), and the oversampling ratio is defined by $f_c/2\text{BW}$, where f_c is the clock frequency (28 GHz) and BW is the code bandwidth (10 MHz).

For a ZOH DAC, the SNDR in the presence of random timing jitter is

$$\text{SNDR}(f_0) \approx 10 \log_{10} \left(\frac{4\text{OSR}(\sin(\pi f_0/f_c))^2}{A(1 - |C(f)|^2)} \right). \quad (12)$$

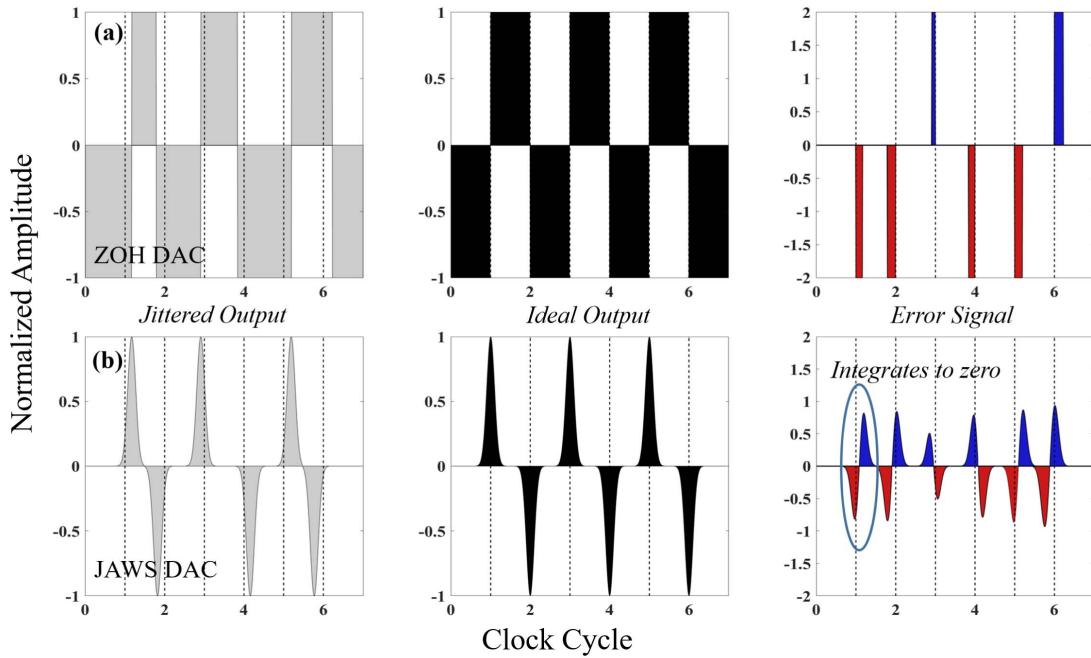


Fig. 10. (a) Output of a ZOH DAC affected by the random timing jitter is broken into the summation of the ideal output and error signal. (b) Output of a JAWS DAC affected by the random timing jitter is broken into the ideal output and error signal. For JAWS, the area of the error signal is always zero over the timescale of a single pulse, which is not true for the ZOH DAC.

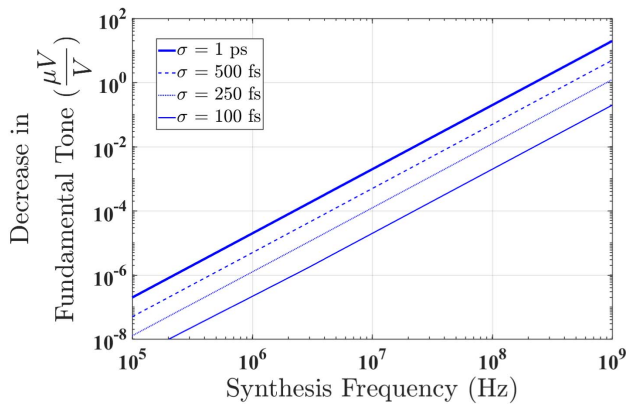


Fig. 11. Decrease in fundamental tone amplitude due to random timing jitter versus frequency. A Gaussian distribution was used to describe the jitter with the standard deviation (σ) of 100 fs–1 ps. We expect $\sigma \approx 250$ fs for the JAWS system.

In Fig. 12, the in-band random jitter-contributed SNDR is shown for a JAWS DAC versus a ZOH DAC for several values of σ in the output frequency range of 100 kHz to 1 GHz and assuming $f_c = 28$ GHz. The target baseline in-band SQNR of the input delta-sigma encoding is also shown.

As discussed, noise due to the random jitter error signal is shaped to high frequencies with the JAWS DAC, and SNDR, therefore, decreases with frequency but is universally higher than the ZOH DAC SNDR in the range of f/f_c shown. In contrast, the noise due to random PWJ for the ZOH DAC more closely approximates white noise, and jitter-contributed SNDR is nearly constant even at frequencies near dc.

C. Verification With Monte Carlo Simulation

To verify the derived random noise power spectrum and SNDR for delta-sigma DACs subject to random PPJ or ran-

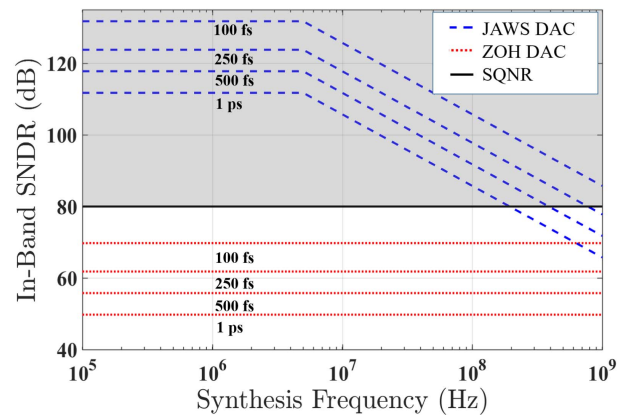


Fig. 12. In-band SNDR due to noise contributed by random timing jitter versus frequency for different values of the standard deviation σ of the jitter distribution. We expect that $\sigma \approx 250$ fs for the JAWS system. The SQNR of 80 dB for the input delta-sigma code is also shown. The SNDR is constant below 5 MHz, because the noise is integrated over a 10 MHz bandwidth.

dom PWJ, we performed Monte Carlo noise simulations. The correspondence between simulated and theoretical noise PSDs in the presence of random timing jitter is shown in Fig. 13.

For these simulations, we first generated an ideal, three-level, 10th-order delta-sigma encoding of a 1 GHz waveform with 100 MHz bandwidth. To simulate PPJ in the JAWS system, each bit in the delta-sigma code was substituted with a SPICE-simulated SFQ pulse waveform. Each pulse was offset by a random value selected from a Gaussian distribution with $\sigma = 1$ ps and mean of 0. For the ZOH DAC simulation of PWJ, the ideal transition times between delta-sigma code levels were perturbed by the same randomly selected time offsets. In both the cases, the process was repeated 70 times, and the resulting power spectra were averaged. To compute PSD,

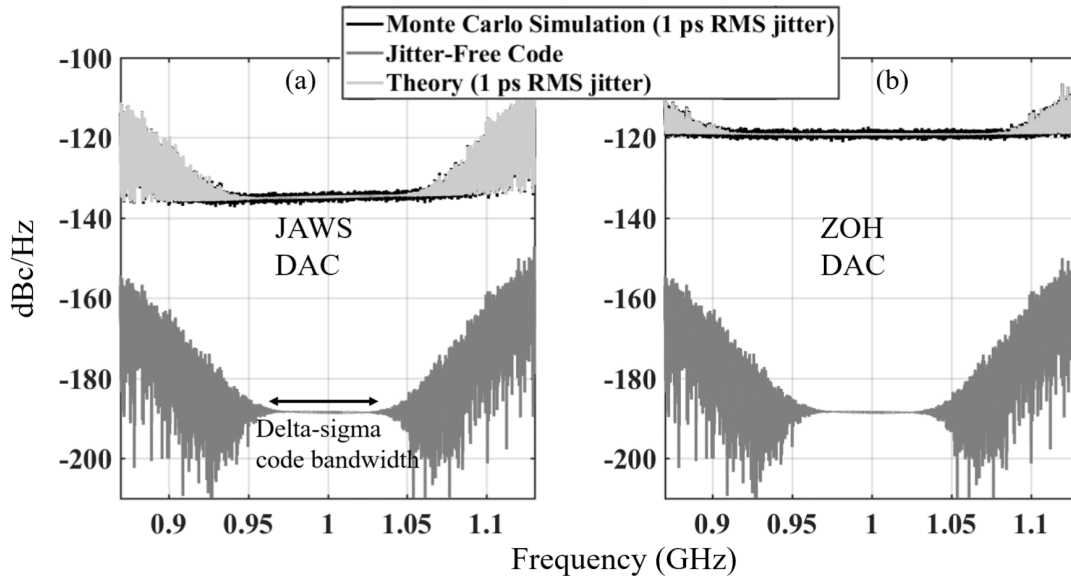


Fig. 13. (a) Comparison between Monte Carlo simulation and theoretical formula for the noise PSD (plotted in dBc/Hz) of a 1 GHz delta-sigma code due to 1 ps rms random PPJ in the JAWS DAC output pulses. The baseline PSD due to quantization noise in the jitter-free code is also shown. (b) Comparison between simulation and theory for the same delta-sigma code, subject to random 1 ps rms PWJ, as in a ZOH DAC output.

we divided the simulated noise power in a given frequency bin by the frequency bin spacing (20.8 kHz in these simulations).

We observed an excellent match between theoretical PSD and simulation results for both PPJ and PWJ, which confirms the validity of the derived expressions in (11) and (12).

V. DISCUSSION

Our simulations of random and deterministic jitter show that the JAWS system can be extended to synthesis above 1 GHz and maintain amplitude accuracy $<2000 \mu\text{V/V}$, assuming that timing jitter is the only source of uncertainty in the system. This result is an important component of an overall JAWS amplitude accuracy analysis.

In reality, other non-jitter-related sources of uncertainty will also be prevalent at microwave frequencies. In particular, before the JAWS system is disseminated as a microwave-frequency voltage standard, additional work is needed to bound the frequency-dependent uncertainty in $P(f)$. While efforts to bound overall uncertainty are ongoing, the JAWS system can be deployed for applications that require a perfectly linear and low-distortion waveform source, provided that we can eliminate sources of deterministic jitter that generate in-band spurious content.

We have shown that unipolar encodings present a potential solution for avoiding I_{dc} -dependent deterministic jitter, although this encoding scheme will reduce the maximum possible amplitude of f_0 by a factor of two. The number of JJs could be doubled to recover the full amplitude, but doubling the array length makes it experimentally difficult to achieve a uniform pulse drive amplitude for all JJs, and standing waves become problematic as the electrical length of the array approaches the synthesis frequency wavelength.

One potential solution is to keep array length constant but to double the number of arrays, and to dedicate each array to a single polarity. This solution would involve driving two arrays with opposite polarity inputs and measuring the difference

between their outputs (e.g., with an on-chip 180° phase shift element followed by a power combiner, both designed for a center frequency of f_0). Such a technique would eliminate the effects of jitter due to $I_{\text{dc}} \neq 0$, but the insertion loss of the additional circuitry would further degrade amplitude accuracy.

Deterministic jitter could also be reduced by decreasing the characteristic pulse time of the JJs by increasing the $I_c R_s$ product. Simulations show that faster junctions have a smaller Δt for a given value of I_{dc} . However, the benefit of faster JJs would only be realized with a faster pulse drive and higher input bandwidth in the pulse delivery system, both of which are RF engineering challenges.

At microwave frequencies, there will be inevitable tradeoffs between single-tone accuracy, spectral purity, output amplitude, and simply restricting the operational quantum-locked space to a smaller range of I_{dc} . We expect that all microwave JAWS circuits will include an array of pulse-quantizing JJs, but additional circuit details can be varied and optimized depending upon the application.

VI. CONCLUSION

Our simulations show that JAWS can theoretically generate single tones up to 1 GHz while maintaining amplitude uncertainty below the $2000 \mu\text{V/V}$ metric currently set by ac rms power calibration services, even in the presence of deterministic and random PPJ. In addition, the complete lack of random output PWJ inherent in the JAWS circuits allows the device to achieve superior random jitter sensitivity relative to ZOH DAC, although this advantage diminishes with higher output frequency unless clock frequency is also increased. Finally, quantized pulse areas do not protect the JAWS system against spurious tone generation due to deterministic PPJ. Deterministic PPJ causes measurable variation in the output waveform over the quantum-locking range and can be eliminated either by changing the circuit architecture or restricting the input polarity.

Future work will include extending the jitter model to frequencies above 1 GHz to consider deterministic and random variations in the shape of the quantized-area output $P(t)$, rather than only variations in its center position. Through analog circuit modeling of JAWS synthesis with $I_{dc} \neq 0$, we have already begun these efforts. Upcoming experimental work includes confirmation of jitter model predictions at 100 MHz and extension of JAWS synthesis to 1 GHz.

Continued verification of experimental data with the modeling and simulation predictions in this paper will move us closer to introduce JAWS as the first microwave-frequency ac voltage reference standard and to report overall frequency-dependent bounds on its accuracy and spectral purity.

APPENDIX

ANALYTICAL TREATMENT OF DETERMINISTIC JITTER

In Section III-B, the output waveform in the presence of polarity-dependent jitter is written as

$$v_{P,jit}(t) = p(t) \otimes \sum_n w[n] \delta(t - nT + \Delta t(I_{dc})w[n]). \quad (13)$$

In the frequency domain, we may write that

$$v_{P,jit}(t) = \sum_{n=0}^{\infty} |a_n| \sin(2\pi f_n t + \phi_n + (2\pi f_n \Delta t)v_p(t)) \quad (14)$$

where ϕ_n and $|a_n|$ are the phase and amplitude of a particular Fourier component in the unshifted output $v_p(t)$. The jittered output is now conveniently expressed as a summation of the frequency components in the original encoding, each of which has been phase-modulated by the function $(2\pi f_n \Delta t)v_p(t)$. The effects of single-tone phase modulation of a single-tone signal are well known; we extend this analysis to multitone modulation of a multitone signal to provide an analytical framework for the effect of deterministic, polarity-dependent jitter on the output spectrum.

The problem, as defined by (14), can be summarized as follows: the output waveform $v_p(t)$ in the absence of jitter contains a sum of sinusoidal terms with frequencies f_n , phases ϕ_n , and amplitudes a_n . When polarity-dependent jitter is present due to $I_{dc} \neq 0$, each tone f_n is modulated by the same waveform $v_p(t)$, scaled by a factor of $2\pi \Delta t f_n$. The modulation waveform $v_p(t)$ contains frequency components f_k with phases ϕ_k and amplitudes a_k , which are in general the same as those in the original output.

The impact of multitone phase modulation on a particular tone f_n is, to first order in a Jacobi–Anger expansion, expressed as

$$\begin{aligned} & \mathbb{I}m\{|a_n|e^{i(2\pi f_n t + \phi_n)}\} \\ & \xrightarrow{\text{Phase Mod}} \mathbb{I}m\left\{|a_n|e^{i(2\pi f_n t + \phi_n)} \prod_k (J_0(a_k 2\pi \Delta t f_n) \right. \\ & \quad \left. + |a_k| \pi f_n \Delta t (e^{i(2\pi f_k t + \phi_k)} - e^{-i(2\pi f_k t + \phi_k)}))\right\}. \end{aligned} \quad (15)$$

As an example, if the output $v_p(t)$ in the absence of deterministic jitter was only composed of frequency components f_0 (the fundamental tone), f_1 , and f_2 , with amplitudes a_0 ,

a_1 , and a_2 and phases ϕ_0 , ϕ_1 , and ϕ_2 , respectively, then the direct impact of phase modulation on the fundamental tone $a_0 \sin(2\pi f_0 t + \phi_0)$ would be

$$\begin{aligned} & \mathbb{I}m\{|a_0|e^{i(2\pi f_0 t + \phi_0)}\} \\ & \xrightarrow{\text{Phase Mod}} \mathbb{I}m\{|a_0|e^{i(2\pi f_0 t + \phi_0)} \\ & \quad \times (J_0(a_0 2\pi \Delta t f_0) + |a_0| \pi f_0 \Delta t (e^{i(2\pi f_0 t + \phi_0)} \\ & \quad \quad - e^{-i(2\pi f_0 t + \phi_0)})) \\ & \quad \times (J_0(a_1 2\pi \Delta t f_0) + |a_1| \pi f_0 \Delta t (e^{i(2\pi f_1 t + \phi_1)} \\ & \quad \quad - e^{-i(2\pi f_0 t + \phi_1)})) \\ & \quad \times (J_0(a_2 2\pi \Delta t f_0) + |a_2| \pi f_0 \Delta t (e^{i(2\pi f_2 t + \phi_2)} \\ & \quad \quad - e^{-i(2\pi f_2 t + \phi_2)}))\} \end{aligned} \quad (16)$$

with analogous expressions holding for the impact of phase modulation on each of the other two spectral components. When expanding the products in (16), to the first order, we ignore the terms of order Δt^2 . Then, it follows that the first-order impact of multitone phase modulation on the fundamental tone is to change its amplitude from $|a_0|$ to:

$$\begin{aligned} & |a_0|(J_0(a_0 2\pi \Delta t f_0) \times J_0(a_1 2\pi \Delta t f_0) \times J_0(a_2 2\pi \Delta t f_0)) \\ & = |a_0| \prod_{f_m} (J_0(a_m 2\pi \Delta t f_0)) \\ & = |a_0|(1 - \alpha(f_0)) \end{aligned} \quad (17)$$

where

$$\alpha(f_0) = 1 - \prod_{f_m} (J_0(a_m 2\pi \Delta t f_0)) \quad (18)$$

which is the same as 6. In this example $m \in 1-3$, however, the result generalizes to an arbitrary number of frequency components. The Bessel function $J_0(x)$ falls below one as its argument grows large, which means that the attenuation of a tone grows with increasing f_n and Δt . Assuming that a_0 is the dominant amplitude in the waveform spectrum, while a_1 and a_2 represent quantization noise in a delta–sigma encoding, the term $J_0(a_0 2\pi \Delta t f_0)$ dominates the attenuation factor. The exact delta–sigma noise shaping properties and corresponding amplitudes of a_1 and a_2 have negligible impact on the overall attenuation.

In addition, (16) indicates that new spectral components are generated from the modulated tone f_0 at frequencies $f_0 + f_0$, $|f_0 \pm f_1|$, and $|f_0 \pm f_2|$, with amplitudes and phases that can be read from the equation. Correspondingly, the phase modulation of frequency component f_1 will generate spectral content at frequencies $f_1 + f_1$, $|f_1 \pm f_0|$, $|f_1 \pm f_2|$, and so on.

The waveform $v_p(t)$ has frequency components at evenly spaced intervals, and their mixing will generate spectral content only within the original frequency grid. For example, if f_1 and f_2 represent the harmonics of f_0 , then new frequency content will be generated at the tone f_1 due to the mixing components $|f_2 - f_0|$, $|f_0 - f_2|$, and $f_0 + f_0$. This is the source of the term $\Delta_{a,m}$ discussed in the main text.

In the particular case that $f_1 = 2f_0$, the spectral component contributed to $\Delta_{a,m}$ by $f_0 + f_0$ is large in magnitude, because its amplitude [as read from (16)] is proportional to $|a_0|^2$, and the fundamental tone amplitude a_0 is, by design orders of magnitude, larger than any other quantization noise tone in the output spectrum. This explains the strong second

harmonic generation discussed in Section III-B3 and shown experimentally in Section III-C2.

For all other tones f_n within the spectral range of interest (up to ~ 1 GHz), the main contribution to $\Delta_{a,m}$ will be mixing of all frequency pairs (f_i and f_j), whose difference $f_j - f_i$ is equal to f_n , rather than additive mixing-up of low-frequency components of $v_p(t)$. If $f_i < f_j$, then the phase modulation of f_i by frequency component f_j generates a sinusoidal signal at frequency f_n with amplitude $|a_i||a_j|\pi f_i \Delta t$ and phase $\phi_j - \phi_i$ [this can be read from (16)]. Similarly, the phase modulation of f_j by frequency component f_i generates a sinusoidal signal at frequency f_n with amplitude $-|a_j||a_i|\pi f_j \Delta t$ and phase $\phi_j - \phi_i$. The net amplitude of these two contributions to $\Delta_{a,m}$ is

$$\begin{aligned} |a_i||a_j|\pi f_i \Delta t - |a_j||a_i|\pi f_j \Delta t &= |a_j||a_i|\pi(f_i - f_j)\Delta t \\ &= -|a_j||a_i|\pi f_n \Delta t. \end{aligned} \quad (19)$$

To find the total magnitude and phase of $\Delta_{a,m}$ from the contribution of all frequency pairs (f_i, f_j), we take the summation over the full spectrum of $v_p(t)$

$$\Delta_{a,m} = \sum_n -\pi f_n \Delta t |a_j||a_i| e^{j(\phi_j - \phi_i)} \quad (20)$$

which explains the average linear scaling of $\Delta_{a,m}$ with f_n and Δt .

ACKNOWLEDGMENT

The authors would like to thank A. Fox for fabricating the JAWS chips used in the experiments and P. Sotiriadis and C. Basetas of the National Technology University of Athens for providing the bandpass delta-sigma encodings that were used for the simulations described in this paper. The authors would like to thank C. Nelson, K. Irwin, B. Murmann, and other colleagues at the National Institute of Standards and Technology (NIST) and Stanford University who advised them on this work. The authors would also like to thank the Boulder Microfabrication Facility and NIST staff who support it.

REFERENCES

- [1] R. Behr, O. Kieler, J. Kohlmann, F. Müller, and L. Palafox, "Development and metrological applications of Josephson arrays at PTB," *Meas. Sci. Technol.*, vol. 23, no. 12, 2012, Art. no. 124002.
- [2] N. E. Flowers-Jacobs, S. B. Waltman, A. E. Fox, P. D. Dresselhaus, and S. P. Benz, "Josephson arbitrary waveform synthesizer with two layers of Wilkinson dividers and an FIR filter," *IEEE Trans. Appl. Supercond.*, vol. 26, no. 6, Sep. 2016, Art. no. 1400307.
- [3] D. Newell *et al.*, "The CODATA 2017 values of h , e , k , and N_A for the revision of the SI," *Metrologia*, vol. 55, no. 1, pp. L13–L16, 2018.
- [4] J. A. Brevik *et al.*, "Radio-frequency waveform synthesis with the Josephson arbitrary waveform synthesizer," in *Proc. 31st Conf. Precis. Electromagn. Meas. (CPEM)*, Jul. 2018, Art. no. CPEM-S776-16-1803092305.
- [5] A. Rüfenacht, N. E. Flowers-Jacobs, A. E. Fox, C. J. Burroughs, P. D. Dresselhaus, and S. P. Benz, "Direct comparison of a pulse-driven Josephson arbitrary waveform synthesizer and a programmable Josephson voltage standard at 1 volt," in *Proc. Conf. Precis. Electromagn. Meas. (CPEM)*, Jul. 2016, pp. 1–2.
- [6] R. Behr, J. M. Williams, P. Patel, T. J. B. M. Janssen, T. Funck, and M. Klonz, "Synthesis of precision waveforms using a SINIS Josephson junction array," *IEEE Trans. Instrum. Meas.*, vol. 54, no. 2, pp. 612–615, Apr. 2005.
- [7] M. Kampik and G. Popek, "The effect of DAC clock jitter on the RMS value of digitally synthesized AC voltage," in *Proc. Conf. Precis. Electromagn. Meas.*, Jul. 2012, pp. 542–543.
- [8] B. Jeanneret, F. Overney, L. Callegaro, A. Mortara, and A. Rufenacht, "Josephson-voltage-standard-locked sine wave synthesizer: Margin evaluation and stability," *IEEE Trans. Instrum. Meas.*, vol. 58, no. 4, pp. 791–796, Apr. 2009.
- [9] H. Tao, L. Toth, and J. M. Khoury, "Analysis of timing jitter in bandpass sigma-delta modulators," *IEEE Trans. Circuits Syst. II, Analog Digit. Signal Process.*, vol. 46, no. 8, pp. 991–1001, Aug. 1999.
- [10] R. Saad, S. Hoyos, and S. Palermo, "Analysis and modeling of clock-jitter effects in delta-sigma modulators," in *MATLAB—A Fundamental Tool for Scientific Computing and Engineering Applications*, vol. 1. London, U.K.: InTech, 2012, ch. 17, pp. 393–422.
- [11] S. M. Taleie, T. Copani, B. Bakkaloglu, and S. Kiaei, "A linear $\Sigma - \Delta$ digital IF to RF DAC transmitter with embedded mixer," *IEEE Trans. Microw. Theory Techn.*, vol. 56, no. 5, pp. 1059–1068, May 2008.
- [12] D. Mercer, "A 16-b D/A converter with increased spurious free dynamic range," *IEEE J. Solid-State Circuits*, vol. 29, no. 10, pp. 1180–1185, Oct. 1994.
- [13] M. Anderson and M. Sundstrom, "DT modeling of clock phase-noise effects in LP CT $\Delta\Sigma$ ADCs with RZ feedback," *IEEE Trans. Circuits Syst., II, Exp. Briefs*, vol. 56, no. 7, pp. 530–534, Jul. 2009.
- [14] O. Oliaei and H. Aboushady, "Jitter effects in continuous-time $\Delta\Sigma$ modulators with delayed return-to-zero feedback," in *Proc. Int. Conf. Electron., Circuits, Syst.*, Sep. 1998, pp. 351–354.
- [15] S. Pavan, R. Schreier, and G. C. Temes, *Understanding Delta-Sigma Data Converters*, 2nd ed. Hoboken, NJ, USA: Wiley, 2017.
- [16] M. Ortmanns, F. Gerfers, and Y. Manoli, "A continuous-time $\Sigma\Delta$ modulator with reduced sensitivity to clock jitter through SCR feedback," *IEEE Trans. Circuits Syst. I, Reg. Papers*, vol. 52, no. 5, pp. 875–884, May 2005.
- [17] M. Tanihata and T. Waho, "A feedback-signal shaping technique for multi-level continuous-time delta-sigma modulators with clock-jitter," in *Proc. 36th Int. Symp. Multiple-Valued Logic (ISMVL)*, May 2006, p. 20.
- [18] H. Chang and H. Tang, "Review and comparison of clock jitter noise reduction techniques for lowpass continuous-time delta-sigma modulators," *J. Low Power Electron. Appl.*, vol. 7, no. 3, 2017, Art. no. 22.
- [19] L. Angrisani and M. D'Arco, "Modeling timing jitter effects in digital-to-analog converters," *IEEE Trans. Instrum. Meas.*, vol. 58, no. 2, pp. 330–336, Feb. 2009.
- [20] J. A. Brevik, N. E. Flowers-Jacobs, A. E. Fox, E. B. Golden, P. D. Dresselhaus, and S. P. Benz, "Josephson arbitrary waveform synthesis with multilevel pulse biasing," *IEEE Trans. Appl. Supercond.*, vol. 27, no. 3, Apr. 2017, Art. no. 1301707.
- [21] B. Baek, P. D. Dresselhaus, and S. P. Benz, "Co-sputtered amorphous Nb_xSi_{1-x} barriers for Josephson-junction circuits," *IEEE Trans. Appl. Supercond.*, vol. 16, no. 4, pp. 1966–1970, Dec. 2006.
- [22] T. Van Duzer and C. W. Turner, *Principles of Superconductive Devices and Circuits*, 2nd ed. Upper Saddle River, NJ, USA: Prentice-Hall, 1998.
- [23] N. E. Flowers-Jacobs, A. E. Fox, P. D. Dresselhaus, R. E. Schwall, and S. P. Benz, "Two-volt Josephson arbitrary waveform synthesizer using Wilkinson dividers," *IEEE Trans. Appl. Supercond.*, vol. 26, no. 6, Sep. 2016, Art. no. 1400207.
- [24] *WRspice Circuit Simulation*, Whiteley Res., Sunnyvale, CA, USA, 1996. [Online]. Available: <http://wrcad.com>
- [25] B. Jeanneret and S. P. Benz, "Application of the Josephson effect in electrical metrology," *Eur. Phys. J. Special Topics*, vol. 172, no. 1, pp. 181–206, 2009.
- [26] T. E. Lipe, J. R. Kinard, Y.-H. Tang, S. P. Benz, C. J. Burroughs, and P. D. Dresselhaus, "Thermal voltage converter calibrations using a quantum ac standard," *Metrologia*, vol. 45, no. 3, pp. 275–280, 2008.
- [27] F. R. Clague, "A calibration service for coaxial reference standards for microwave power," NIST, Gaithersburg, MD, USA, Appl. Note 1374, 1995.
- [28] M. Z. Win, "On the power spectral density of digital pulse streams generated by M-ary cyclostationary sequences in the presence of stationary timing jitter," *IEEE Trans. Commun.*, vol. 46, no. 9, pp. 1135–1145, Sep. 1998.
- [29] K. Doris, A. van Roermund, and D. Leenaerts, "A general analysis on the timing jitter in D/A converters," in *Proc. Int. Symp. Circuits Syst. (ISCAS)*, vol. 1, May 2002, pp. I-117–I-120.
- [30] Y.-K.-K. Fung, G. W. Gibson, J. F. Bulzacchelli, S. Polonsky, and M. B. Ketchen, "Direct measurement of jitter in a JTL," *IEEE Trans. Appl. Supercond.*, vol. 23, no. 3, Jun. 2013, Art. no. 1701405.
- [31] R. McDermott and M. G. Vavilov, "Accurate qubit control with single flux quantum pulses," *Phys. Rev. Appl.*, vol. 2, Jul. 2014, Art. no. 014007.